Middle East Journal of Applied Sciences
Volume: 13 | Issue: 03| July –Sept. | 2023

EISSN: 2706 -7947 ISSN: 2077- 4613
DOI: 10.36632/mejas/2023.13.3.29
Journal homepage: www.curresweb.com
Pages: 441-457

# Mineralization Styles and Alteration Paragenesis of Metasomatic Zones in the Highly Fractionated Granite of Gabal Gattar, Northern Eastern Desert, Egypt

**Amr A. Abdel Hamid, Hicham M. Abdel Hamid, Seddik H. Seddik and Mohamed Metwally**

Nuclear Materials Authority, P.O. 530 El-Maadi, Cairo, Egypt
**Received:** 05 August 2023 **Accepted:** 10 Sept. 2023 **Published:** 20 Sept. 2023

## ABSTRACT

The Gattar-II uranium occurrence is one of the major seven granite-related uranium localities in Gabal Gattar area, northern Eastern Desert of Egypt. It is the most significant occurrence in the area, where many uranium showing were delineated within a metasomatized granitic body, accompanied by many alteration features. This occurrence was selected in this study with the aim to determine the geological, structural and mineralogical characteristics of the uranium mineralization related to metasomatized rocks and construct a paragenetic sequence for the alteration assemblage. The granite at this locality is alkali feldspar granite that belongs to uranium-bearing granite with highly evolved characteristics. The richest uranium ore bodies are distributed along a nearly E–W striking shear zone that transected by mineralized NS, NNE to NE and NW trending fractures. A metasomatic zone is developed along intersections of these fractures with the major shear zone. Main uranium mineralization, predominantly, consisting of uranophane with lesser amounts of pitchblende. Mineralogical and petrographical observations for mineralized samples from G-II suggested at least three stages for alteration and uranium minerals generation in the granite. The earliest pre-ore stage is characterized by partial to complete chloritization of biotite and precipitation of calcite in vugs as well as partial dissolution of primary quartz. This stage is followed by main ore stage, which characterized by local crystallization of pitchblende-pyrite-magnetite assemblage and accumulation of uranophane-fluorite-calcite mineral phases. The last stage of alteration is marked by limited alteration of magnetite to hematite and limonite as well as kaolinitization and precipitation of Mn-oxides.

***Keywords:*** Gattar granite, Alteration paragenesis, Metasomatism, Uranium mineralization, Fluorite.

## 1. Introduction

The uranium mineralization of Gabal Gattar area was explored by the Egyptian Nuclear Materials Authority (NMA) during a ground radiometric survey and follow-up of anomalies in the northern parts of the Gattar batholith. Following this exploration, many researchers have contributed to geological knowledge of this area. Previous studies focused principally on the geology and structures of the ore bodies were described in details by many authors (e.g. Shalaby, 1990, 1995 and 1996; Roz, 1994; Abu Zied, 1995; Haridy, 1995; Abdel Hamid, 2006; El Sundoly and Waheeb, 2015; El Kholy *et al.,* 2019). Contributions to mineralogy and geochemistry of the uranium mineralization have been completed by Mahdy *et al.,* (1990), Sayyah and Attawiya (1990), Khazback *et al.,* (1995), Khalaf (1995), Mahdy (1999), El Kammar *et al.,* (2001), Dawood (2003), Abdel El Hamid (2006), Raslan (2009), Mahdy (2014) and Mahdy *et al.,* (2015).

The uranium ore bodies are hosted by Gabal Gattar granite at its northern peripheries. There, the oldest Hammamat sediments show sharp contact with this granite and host a perigranitic uranium occurrence (Gattar-V occurrence). The other uranium localities are related to the granite itself. The prospect was subjected to small and large scale mining for uranium, including different shapes of excavations such as tunnels, open pits and surface trenches. The most significant uranium ore bodies occur in Gattar-II (G-II) uranium occurrence that was selected in this study. It constitutes one of the

**Corresponding Author:** Amr Abdel Aty Abdel Hamid, Nuclear Materials Authority, P.O. 530 El-Maadi, Cairo, Egypt. E-mail: amr_ahamid@yahoo.com

major seven granite-related uranium occurrences in the area. G-II contains metasomatized granitic ore body, which display different shapes of wall-rock alteration features. The aim of this paper is to represent the results of studies dealing with geology, petrography and mineralogy of metasomatic zones from this locality. Mineral composition and microscopic texture of selected samples are described with the aim to determine the paragenetic sequence of the alteration product.

## 2. Geological Background

### 2.1. Regional Geological Setting

The Gattar batholith locates in the northern part of the northern Eastern Desert of Egypt (Fig. 1a), 40km west of Hurghada city (latitudes 26°51'25"N 27°8'52"N and longitudes 33°13'00"E, 33°25'59"E). It is surrounded by metavolcanics, orogenic older granitoids and the Hammamat sediments of molasse type (Fig. 1b). It shows sharp intrusive contacts against these older rocks. The metavolcanics are exposed in the center of the batholith as roof pendants over the Gattar granites at Gabal Kehla. They are consisting of metabasalts and metadolerites (Abu Zied, 1995). The orogenic older granitoids are surrounded the batholith as low to moderated outcrops and contain diorite, quartz diorite and granodiorite (Roz, 1994). The Hammamat sediments are covering the northern regions of Gabal Gattar area. They are forming the southern extension of Gabal Um Tawat. These rocks comprise greenish and brownish siltstone and greywack interbedded with minor conglomerate (Holail and Moghazi, 1998).

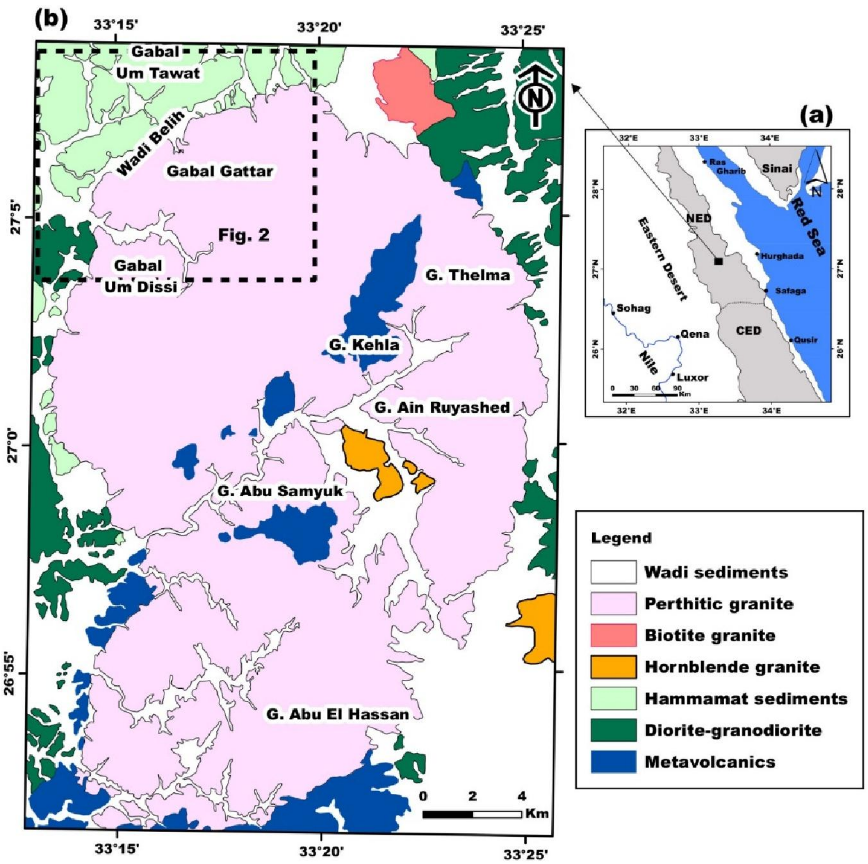


**Fig. 1:** Geological map showing the lithotectonic units of Gabal Gattar area, northern Eastern Desert, Egypt.

The Gattar batholith granitic rocks are equivalent to younger granites and post orogenic plutonites of Egypt (El Ramly and Akaad, 1960; Akaad and Noweir, 1969&1980). They form series of highly elevated mountains with sharp rugged peaks and steep walls. These granites are generally medium-grained, ranging in color from light pink to red or become reddish brown along fault zones as a result of alterations. They are transected by numerous faults and fractures trending mainly to the NNE and

NW directions. There, these rocks become highly hematatized and silicified. Along the fault zones and contacts, the granite shows signs of strong crushing and mylonitization and nearly displaced by NNW faults. Numerous basic dikes of variable attitudes, dimensions and compositions are penetrating the Gattar batholith trending NS, NE and ENE, while acidic dikes are seen cut only the oldest rocks.

**2.2. Local Geology of G-II Occurrence**

The northern segment of Gabal Gattar area contains many uranium showings of lensoid ore bodies grouped into seven uranium occurrences (Gattar-I to Gattar-VII), extending over some few kilometers along the northern faults (Fig. 2). They are predominantly localized in the highly fractionated alkali feldspar granite of the northern peripheries of the Gattar batholith and are also encountered along the contacts with the Hammamat sediments in G-V occurrence. These ore bodies are controlled by tectonic structures mostly represented by strike-slip faults and shear zones along which hydrothermal alteration is developed.

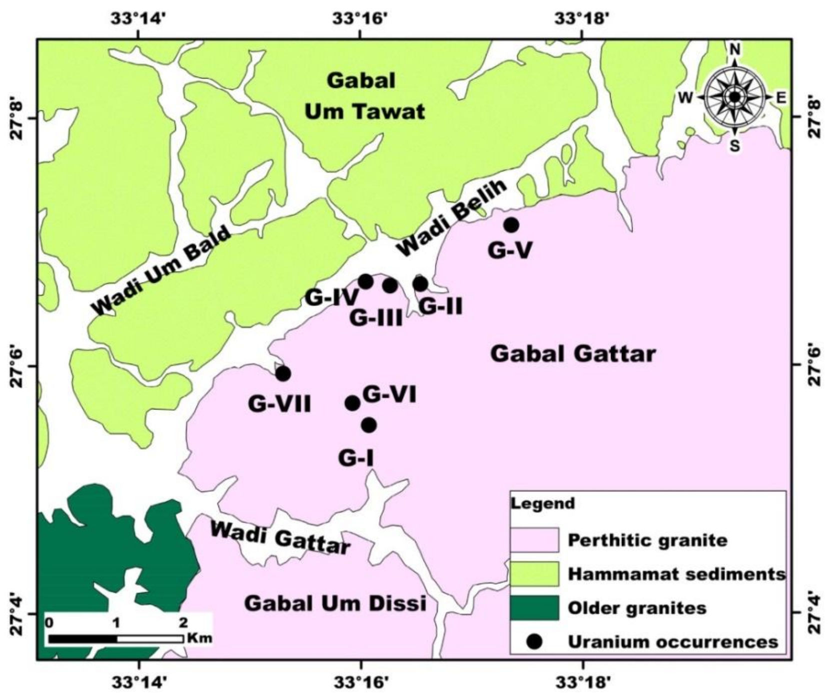


**Fig. 2:** Geological map of the northern region of Gabal Gattar area illustrates the locations of the seven uranium occurrences.

The granite at G-II occurrence is a perthitic granite of late Proterozoic age, with their associated basic dikes and quartz veins. It forms triangular granitic block with high relief and sharp rugged peak (Fig. 3). This granite is highly sheared and dissected by numerous faults and fractures. It is medium-grained and range in color from pink or slightly red to dark or reddish brown depends mainly on the type of alteration. Various types of post-magmatic alterations are widespread around the uranium mineralization. This granite is dissected by numerous quartz veins and veinlets as well as basic dikes. The mining activity in G-II uranium occurrence includes two tunnels, mine shaft, small trenches and large open pit with different dimensions and heights. They cover the eastern and western sides of the occurrence and located entirely in a major E-W highly radioactive and altered zone (Fig. 4).

*Middle East J. Appl. Sci., 13(3): 441-457, 2023*
*EISSN: 2706 -7947 ISSN: 2077- 4613* *DOI: 10.36632/mejas/2023.13.3.29*

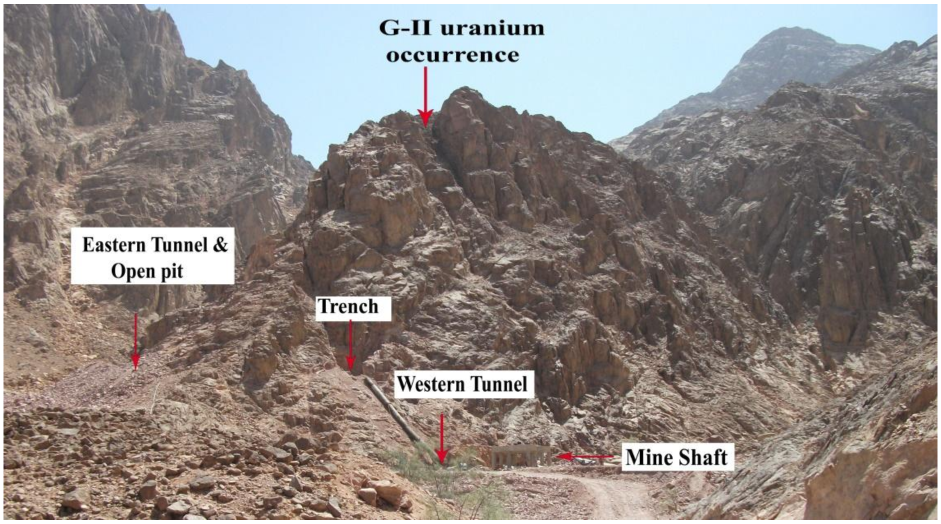


**Fig. 3:** Field photograph showing the G-II uranium occurrence forms highly elevated mountain with sharp rugged peak.

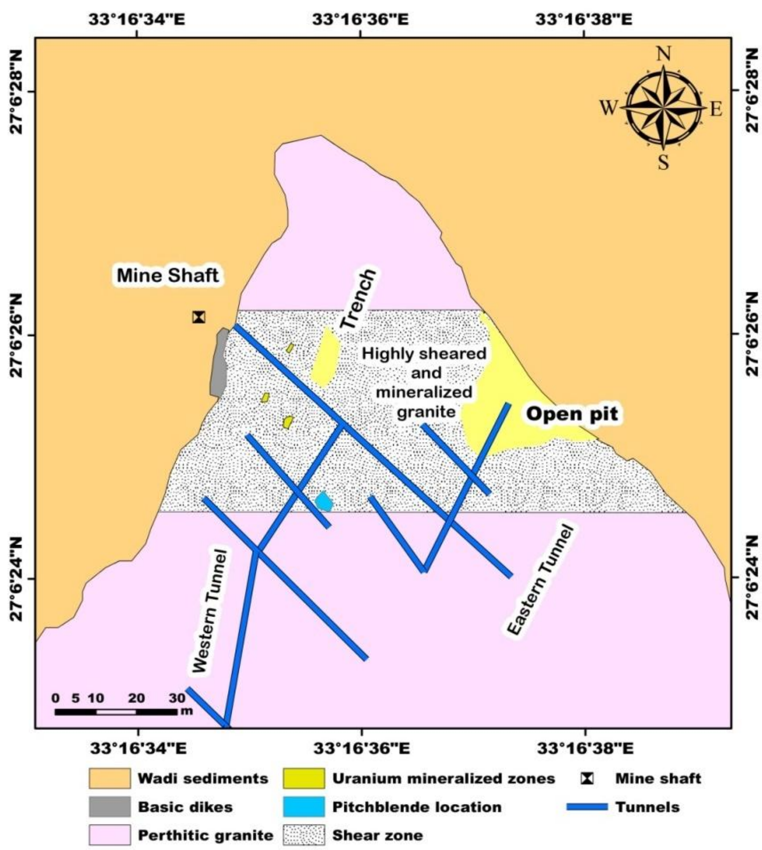


**Fig. 4:** Geological map of G-II uranium occurrence, showing the locations of tunnels, open pit and surface trenches.

## 2.3. Mineralization Styles and Alteration Features

The uranium mineralized bodies of G-II occurrence found as discontinuous lenses grouped into two zones extending over some hundreds of meters in the granite. The uranium minerals include uranophane with its beta modification and local crystallization of pitchblende (Fig. 5a & b). Pitchblende was documented inside the western tunnel of the studied occurrence (Shahin, 2014). It is amorphous in shape, dense and black in color and occurs as patches. Other metals such as pyrite and magnetite are also enriched in this altered domain. Generally, the wall-rock alterations in this locality mainly include silicification, fluoritization, carbonatization, kaolinitization and hematatization. Each type of these alterations can be seen individually or may associates with the other alteration phases. Silicification is commonly represented by quartz veins and veinlets intersected the granite as well as filling pore spaces between major minerals in mineralized samples (Figs. 5c&d). The silicification process is mainly resulting from strong acidic hydrothermal solutions with temperature ranging between 300$^{O}$C and 400$^{O}$C (Burnham, 1962).

Fluoritization is usually found in the center of the ore bodies, forming the fluorite-type ore in the eastern sector of G-II occurrence. It is predominantly forms abundant veins cross-cutting the rock or as discrete grains filling cavities in the mineralized granite (Figs. 6a &b). The development of the fluorite veining displays a close spatial association with the mineralized fractures. Hematatization is usually shown with the uranium mineralization (Fig. 6c), forming one of the main wall-rock alterations in Gabal Gattar area. It is known that hematatization is caused by the redox reaction between oxidized uranium bearing fluid and reduced component of host rocks (Rich *et al.,* 1977; Langmuir, 1978). However, not all hematatized rocks in G-II occurrence are mineralized (Fig. 6d). The initial hematatization is generally barren, and locally gives the granite a distinctive brick-red coloration. The hematitic alteration and associated mineralizations are overprinted by kaolinitic alteration, which is, in turn, locally overprinted by Mn-oxides. The Mn-oxides are pervasive in the barren and mineralized granite. Some samples of the less altered granite are seen stained by manganese dendrites (Fig. 7a) or in some cases filling the microfractures of the rock (Fig. 7b). Alteration of biotite to chlorite is usually observed in the barren granite. The intensity of this process is increased in the highly deformed and mineralized granite and may occur as fracture-filling besides kaolinite (Fig. 7c). Epidotization is registered also in the mineralized samples (Fig. 7d).

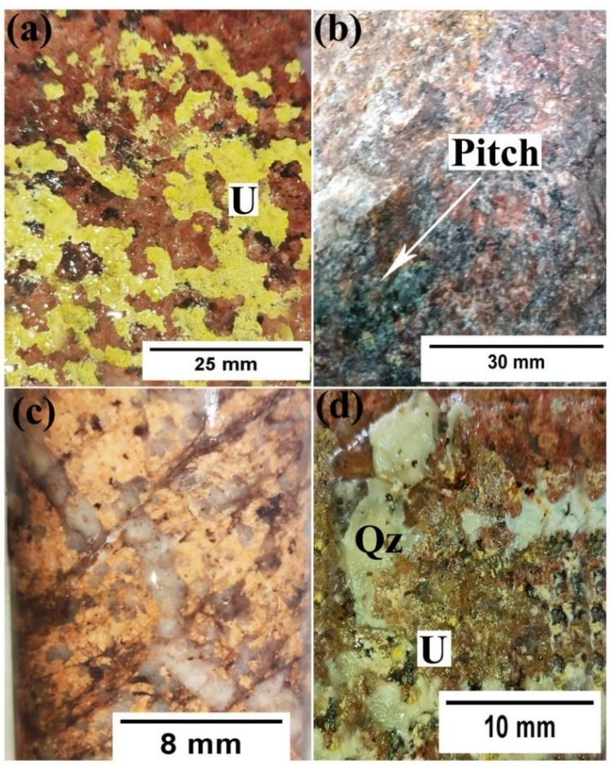


**Fig. 5:** Photographs of mineralization and metasomatic alterations in G-II occurrence, (a) Uranophane, (b) Patches of pitchblende, (c) Displaced quartz veins, and (d) Quartz filling cavities and associates spotty uranophane. U: uranophane, Pitch: pitchblende, Qz: quartz.

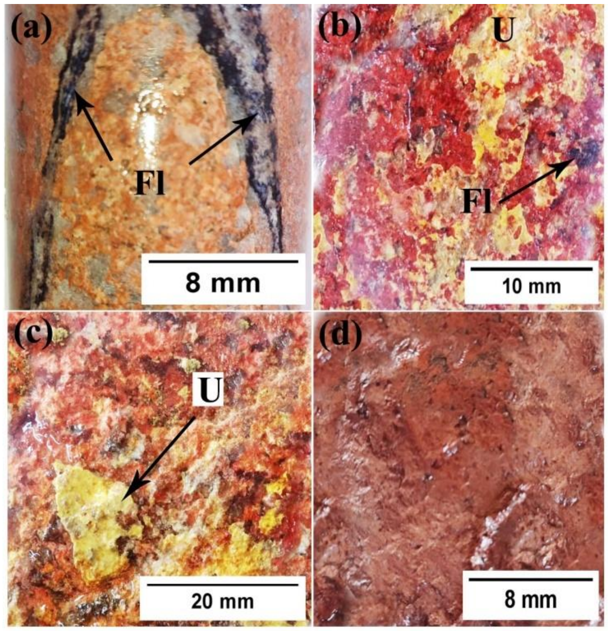


**Fig. 6:** Photographs of the mineralization and associated alterations in G-II occurrence, (a) Veinlets of violet and dark violet fluorite, (b) Discrete crystals of fluorite associates uranophane, (c) Hematite associates uranophane, and (d) Completely hematatized barren granite. U: uranophane Fl: fluorite.

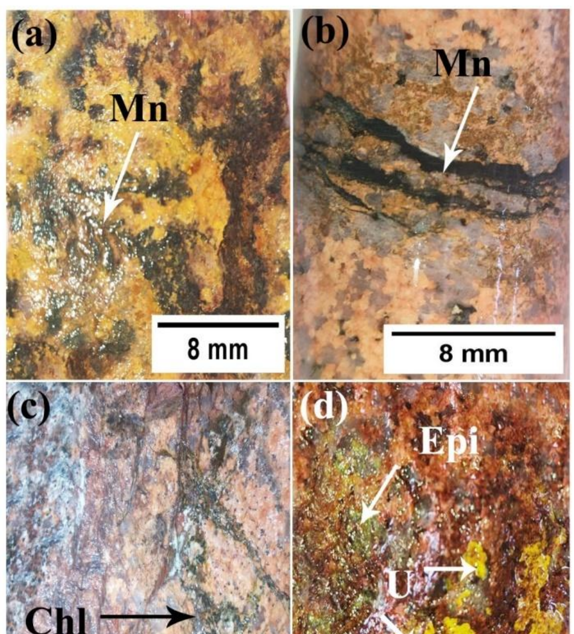


**Fig. 7:** Photographs of the wall-rock alterations in G-II occurrence, (a) Manganese dendrites (Mn) staining the rock surface, (b) Fracture-filling Mn-oxides, (c) Chlorite (Chl) is filling microfracture of the granite accompanying kaolinite, and (d) Epidote associates uranophane (U) and hematite. Mn: manganese oxides, Chl: chlorite, Epi: epidote, U: uranophane.

**2.4. Structural Control of Mineralization**

The localization of uranium mineralization along the fault and fracture zones is a characteristic attribute of Gabal Gattar uranium prospect. The structural studies on the uranium ore bodies from Gattar area were pointed out in almost all publications by the researchers from the Nuclear Materials Authority of Egypt and others (e.g. El Rakaiby and Shalaby, 1988; Shalaby, 1990, 1995, 1996; Roz, 1994; Abu Zied, 1995; Hariedy, 1995; El Kholy, 2012; El Sundoly and Waheeb, 2015; El Kholy *et al.,* 2019). It is clear that the most important factor controlling the deposition of uranium in this district is the occurrence of large tectonic zones, which became the paths of circulation and discharge of uranium-bearing hydrothermal solutions in the northern zones of Gattar batholith. G-II uranium occurrence is bounded by two shear zones (Fig. 8). The first shear zone is striking N12$^0$E that represents the east extension of G-VI shear, while the second one is trending N55$^0$W that bound the mass from the east. Inside the granitic body, the uranium mineralization is controlled by earlier E-W shear zone that was transected later by smaller NS, NE to NNE and NNW strike-slip faults. Intersections of these trends are usually display extensive alterations and mineralization. In some cases, the fault zone is filled by breccia (Fig. 9a) or the granite itself is being brecciated, where many alteration types are developed. The brecciated granite is always filled by hematite between its grains (Fig. 9b).

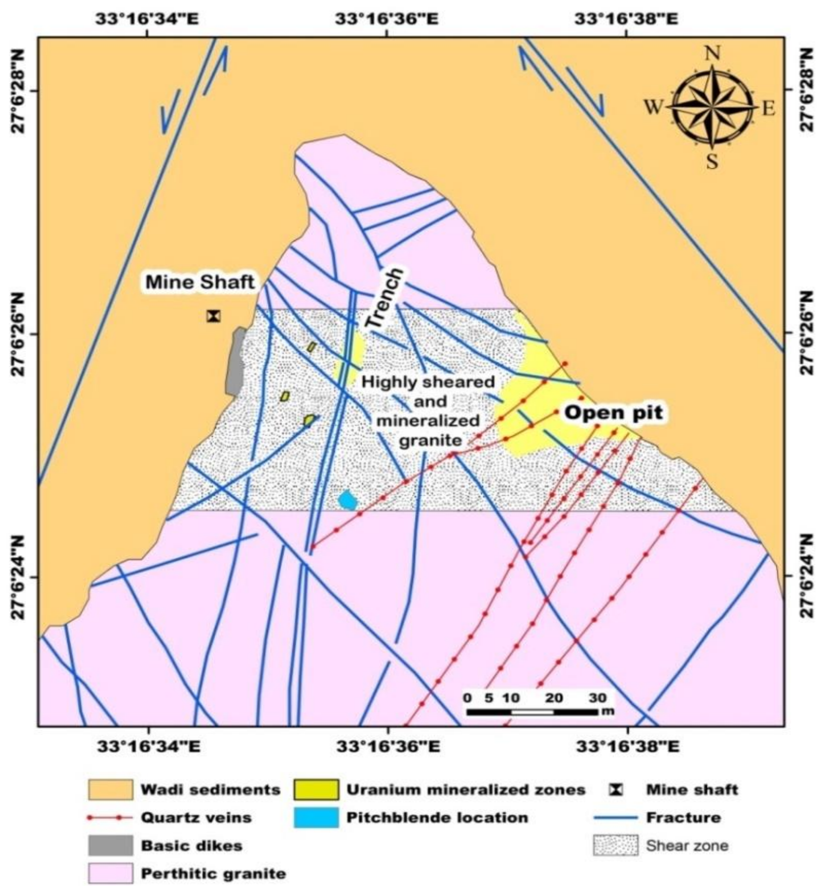


**Fig. 8:** Structural map of G-II uranium occurrence.

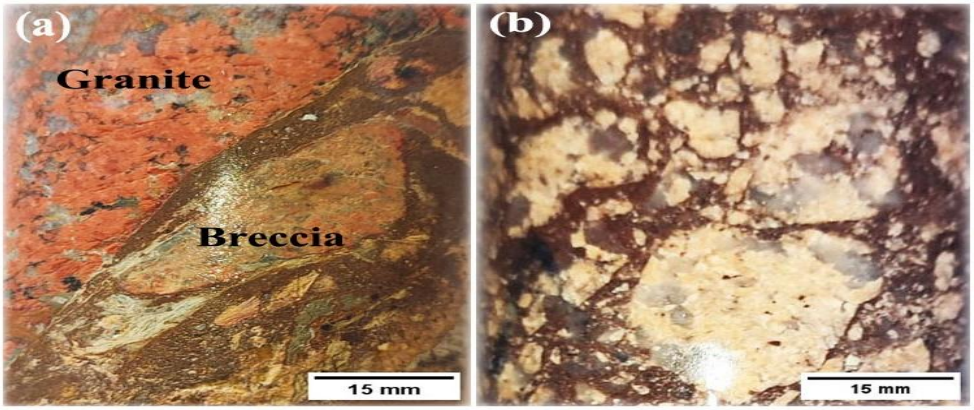


**Fig. 9:** Photographs showing, (a) Contrast between unaltered granite and fault breccia, and (b) Brecciation of the Gattar granite followed by precipitation of hematite between its grains.

## 3. Sampling and Methods

Less altered granite and its corresponding hydrothermally altered varieties were sampled from outcrops, underground tunnels and surface trenches as well as open pit, which were constructed by the NMA. Samples were selected from the less altered granite, through the ore bodies and metasomatic zones. Thin sections were prepared and petrographic studies were investigated using optical microscope and scanning electron microscope (model Philips XL 30) at the NMA.

## 4. Results

### 4.1. Petrography and mineralogy of alteration assemblage

The granite at G-II occurrence was affected by many alteration features nearly close to the formation of uranium mineralization. Petrographic examination of selected samples from this altered granite, demonstrates the complexity and intergrowth of the various alteration phases in the rock. The alteration paragenesis was determined based on optical microscopy and SEM observations (Table 1). The microscopic studies indicated that the mutual texture, structural relations and replacement features are important during determination of the sequence of alteration.

#### 4.1.1. Initial granite and pre-ore alteration

The initial granite shows petrographic features of perthitic leucogranite. It is medium-grained, hypidiomorphic-granular, and dominated by K-feldspar (perthite) and quartz, with minor plagioclase and biotite, as well as alteration product of white mica. The accessory minerals include zircon, apatite, fluorite and magnetite. Biotite occurs as aggregates intergrown with fluorite and is strongly pleochroic from yellow-brown to blue-green. Along fault zones, this granite is altered and reddened. Here, plagioclase is sericitized (Fig. 10a), quartz is recrystallized (Fig. 10b) and biotite is partly replaced by chlorite (Figs 10c). Calcite also occurs in the less altered granite and filling vugs between the major minerals (Fig. 10d). Zircon is metamicted and muscovite found as replacement of K-feldspar (Fig. 10e).

#### 4.1.2. Main-ore stage

At this stage, the uranium minerals are precipitated from the hydrothermal fluids accompanied many complex alteration features. Pitchblende is formed along fault zone in highly altered and brecciated granite in the western sector of G-II occurrence. In contrary, uranophane is widespread in the eastern side of G-II occurrence in the open pit. The mineralized rock is ranging from slightly to moderately and highly altered.

*Middle East J. Appl. Sci., 13(3): 441-457, 2023*
*EISSN: 2706 -7947 ISSN: 2077- 4613* *DOI: 10.36632/mejas/2023.13.3.29*

**Table 1:** Mineral paragenesis of alteration assemblage in G-II metasomatized granite established based on optical and scanning electron microscopes.

| Minerals | Initial granite | Pre-ore alteration | Main ore stage: Pitchblende-pyrite assemblage | Main ore stage: Uranophane-fluorite-calcite assemblage | Oxidation stage |
|---|---|---|---|---|---|
| | Early → | | | | Late |
| K-feldspar | — | | | | |
| Magmatic quartz | — | | | | |
| Plagioclase | — | | | | |
| Biotite | — | | | | |
| Magnetite | — | | — | | |
| Sphene | — | | | | |
| Zircon | — | | | | |
| Fluorite | — | | | — | |
| Apatite | — | | | | |
| Chlorite | | — | | | |
| Muscovite | | — | | | |
| Epidote | | — | | | |
| Sericite | | — | | | |
| Secondary quartz | | — | — | — | |
| Pyrite | | | — | | |
| Pitchblende | | | — | | |
| Calcite | | — | — | — | |
| Uranophane | | | — | — | — |
| Hematite | | | — | — | — |
| Kaolinite | | | | | — |
| Limonite | | | | | — |
| Mn-oxides | | | | | — |

The widths of lines indicate relative abundances of minerals.

#### 4.1.2.1. Pitchblende-pyrite assemblage

These patchy zones of radioactivity consist of a complex intergrowth of pitchblende-pyrite-magnetite mineral phases. Calcite and hematite are also seen with this assemblage. Pitchblende is locally observed as patches interstitial of the major minerals or filling the cracks of the rock (Fig. 11a). ESEM image and element map of pitchblende are shown in Figs. (11b&c). EDX analysis of pitchblende is illustrated in Figs. (11d&e). In addition, some pitchblende occurs near pyrite that occurs as discrete euhedral to subhedral crystals disseminated in the rock. Representative ESEM image and its corresponding EDX analysis of pyrite grain are shown in Fig. (12a). In some instances, pitchblende is surrounded and/or overprinted by uranophane. In areas surrounding the mineralization, the granite shows evidence of brittle deformation in the form of microscopic brittle fracturing and associated cataclasis. These zones of increasing permeability are invaded by the mineralizing fluids, but not all zones of brecciation and hematite alteration carry uranium mineralization. Locally, fractures filled with calcite crosscut the mineralized hematite-filled fractures and associated with brecciation (Fig. 12b). In this stage, hematite is prevails and accompanied by hydrothermal magnetite (Fig.12c).

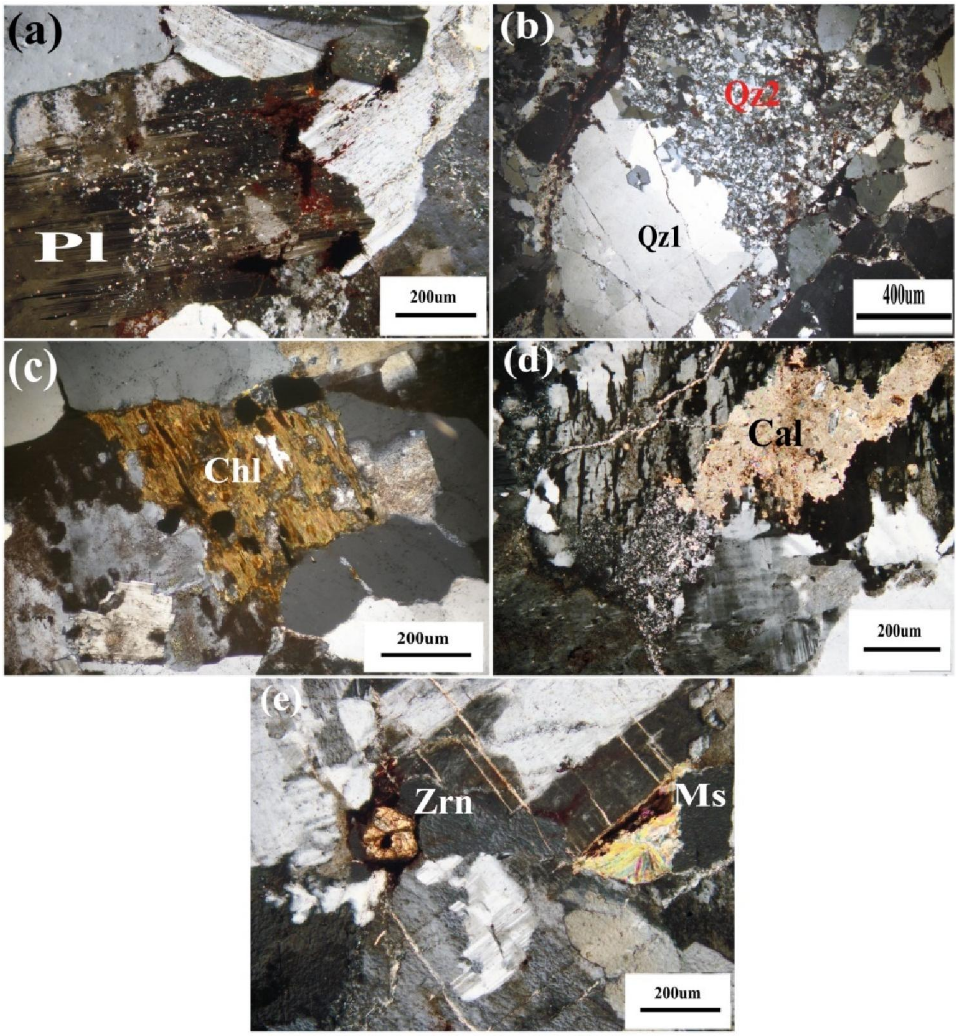


**Fig. 10:** Microphotographs describe the mineral composition of initial Gabal Gattar granite and the principle alteration features in the pre-ore stage, (a) Sercitization of plagioclase, (b) Recrystallized quartz, (c) Biotite completely altered to chlorite, (d) Precipitation of carbonates and secondary silica between pore spaces of major minerals, and (e) Metamictization of zircon. Pl: plagioclase, Qz1: magmatic quartz, Qz2: Secondary silica, Chl: chlorite, Cal: calcite, Zrn: zircon, Ms: muscovite.

***EISSN: 2706 -7947 ISSN: 2077- 4613*** ***DOI: 10.36632/mejas/2023.13.3.29***

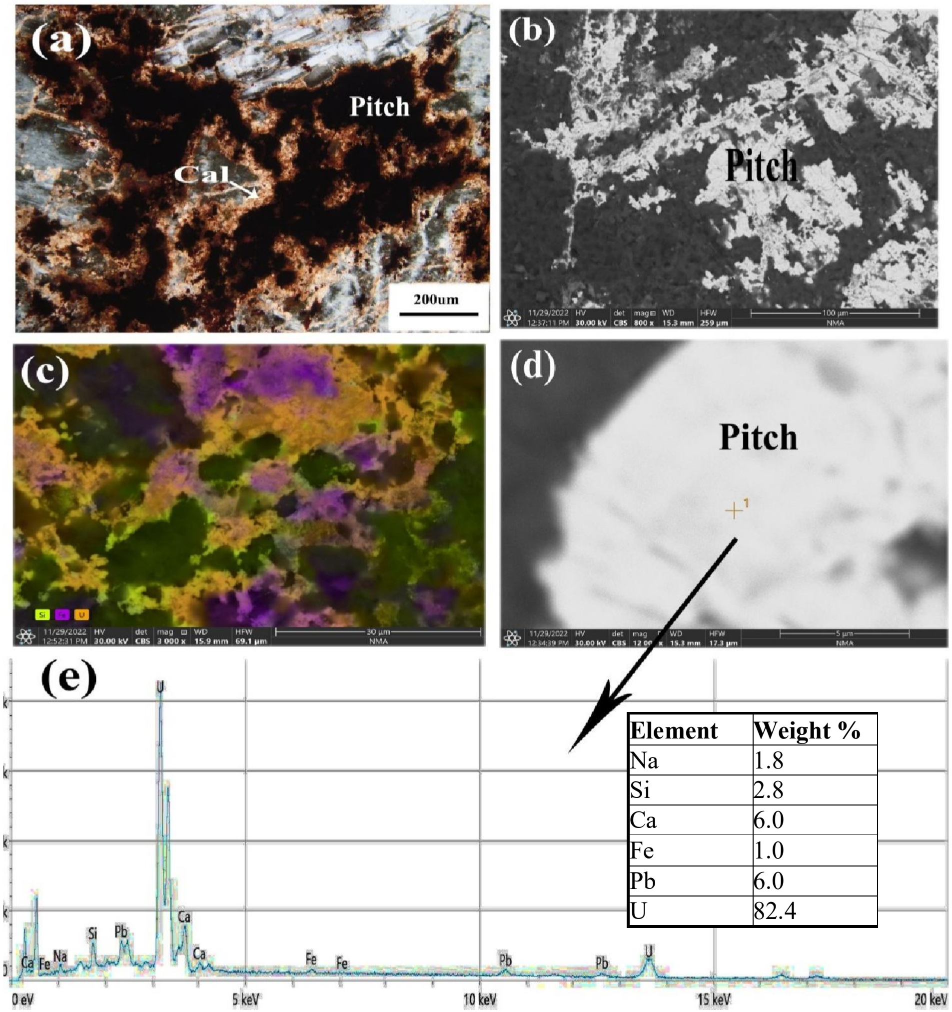


**Fig. 11:** Photomicrographs illustrate the mineralogical characteristics of pitchblende, (a) Patches of pitchblende under the transmitted light, (b) ESEM image of the same photo, (c) elemental map of pitchblende, (d), (e) ESEM image and EDX analysis of pitchblende. Pitch: pitchblende, Cal: calcite.

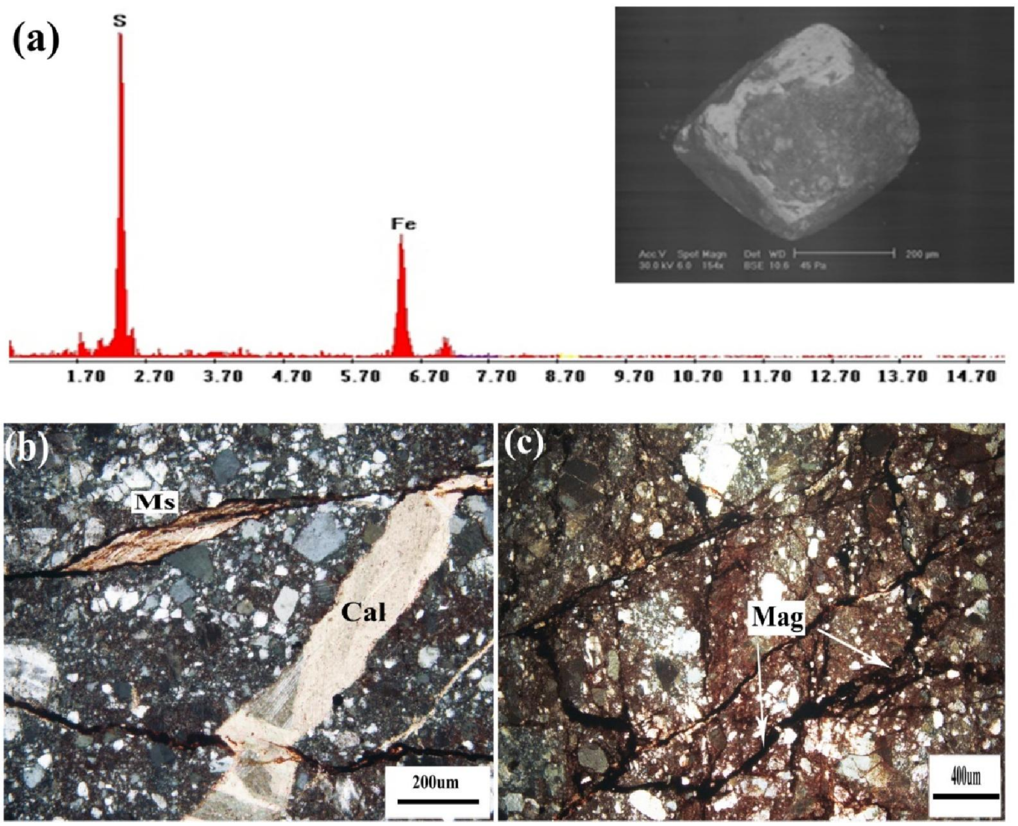


**Fig. 12:** (a) ESEM image and EDX analysis of pyrite mineral grain, (b) Brecciated granite cut by veinlet of calcite and muscovite, and (c) Hematite prevails in the groundmass of brecciated granite and hydrothermal magnetite filling the microfractures of the rock. Cal: calcite, Mag: hydrothermal magnetite, Ms: muscovite.

**4.1.2.2. Uranophane-fluorite-calcite assemblage**

This mineralization assemblage is characterized by the precipitation of disseminated and vug-filling uranium minerals of secondary origin. Uranophane was formed within the secondary pore spaces between major minerals or filled the cracks throughout the minerals. The dissolution of magmatic quartz leaving vugs and uranophane is shown filling these areas (Fig. 13a). ESEM image and its corresponding EDX analysis of uranophane grains are illustrated in Fig. (13b). Large amounts of recrystallized quartz are always associated with uranophane. In some mineralized samples, veinlets of quartz were found crosscutting all existing minerals. They have pinkish gray color with anhedral granular texture and locally display deformation. In this stage, K-feldspar is strongly altered. Abundant fluorite veinlets occur together with calcites are observed in this mineralized stage, which are enclosed by hematatized rock (Fig. 13c). Previous geochemical exploration of these fluorite veins indicated that they enriched with U and REE, which providing evidence that uranophane and fluorite are precipitated together from the same mineralizing solutions (Mahdy, 2014). Dissemination of pale-pink, to orange hematite is observed within the brecciated granite that contains fragments of anhedral to subhedral quartz. This alteration package demonstrates the intensity and duration of hydrothermal activity within the system. Zircon and apatite, which represent the most important accessory minerals in this granite, were subjected to slight changes as a result of hydrothermal reworking.

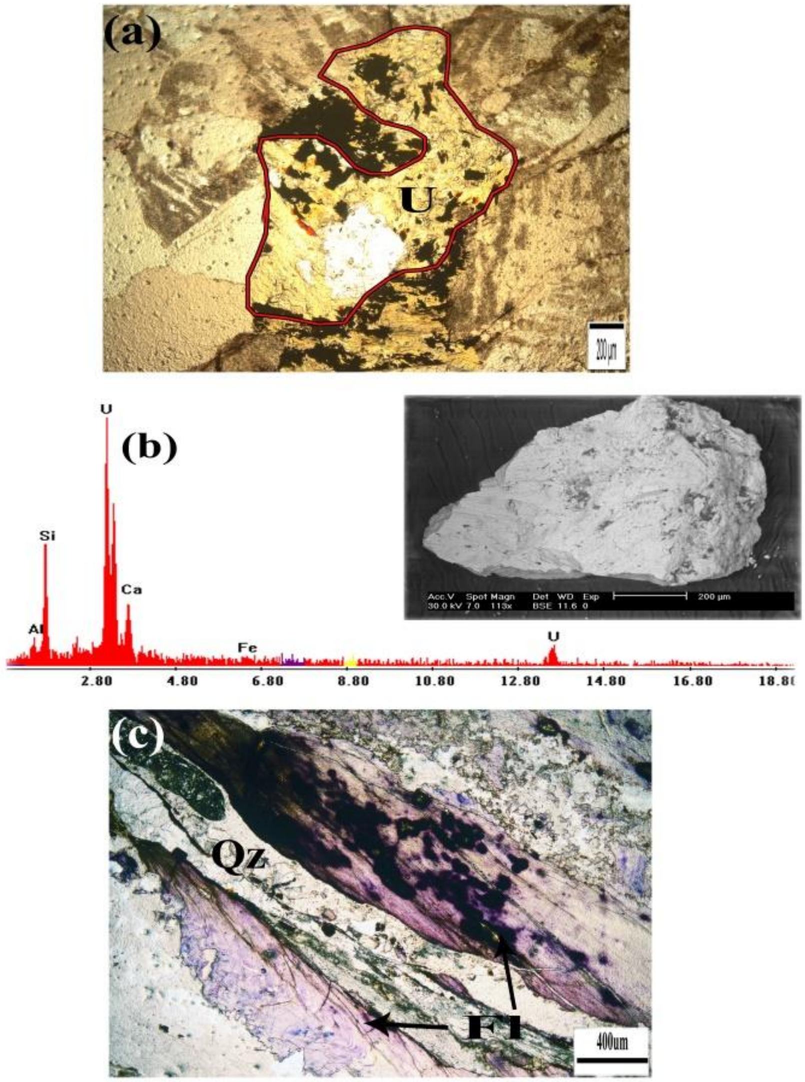


**Fig. 13:** Photomicrographs illustrate the uranophane and associated minerals, (a) Uranophane filling the interstial spaces between common minerals, (b) ESEM image and EDX analysis of uranophane, and (c) Veinlets of violet fluorite associate fracture filling quartz. U: uranophane, Fl: fluorite, Qz: quartz.

### 4.1.3. Late oxidation stage

The late oxidation stage is possibly corresponding to superficial weathering, which includes restricted alteration of magnetite to hematite and limonite. The first stage of hematatization is manifested by slight reddening of K-feldspar and through the alteration of biotite to chlorite. With intense alterations, hematatization is raised and clearly overprints all the pre-existing minerals. Hematite grains are generally quite small and surround the quartz grains, diking the altered rocks into red color. Kaolinitization are coexisting with hematatization in many granitic samples, while Mn-oxides are overprint all these minerals.

## 5. Discussion and Conclusions

The chemical alteration of granitic rock in crustal conditions consists of the dissolution of mineral phases which are unstable under the pertinent conditions of temperature and pressure. This first step is usually followed by a stage where both dissolution of parent minerals and precipitation of neogenic phases are concomitant when relevant conditions of super-saturation occur (Seimbille *et al.,* 1998).

Based on our petrographic work and previous researches (e.g. Mahdy, 1999; El Kammar *et al.,* 2001, Dawood, 2003, Abdel El Hamid, 2006; Mahdy *et al.,* 2015), uranium mineralization of G-II occurrence is irregularly distributed in most metasomatic zones but rich ores occur in the most intensively deformed zones. The common types of alterations associated uranium mineralization in the granite are represented by partial dissolution of quartz (desilicification), sericitization of feldspars, chloritization of biotite, muscovitization, carbonization, kaolinitization and hematatization. Newly formed phases such as fluorite, pyrite and magnetite are also encountered in the altered domain. However, all these alterations are of considerable importance for understanding the physicochemical controls of the hydrothermal solutions affecting Gattar granite.

The hydrothermal activity started with an alkaline and oxidizing hot aqueous medium that caused series of subsolidus alterations evidenced by the partial dissolution and precipitation of carbonates. Chemically silica dissolves only in alkaline medium and carbonates require pH between 7.5 and 7.8 (Krauskopf, 1982). The alkaline solutions dissolve primary quartz according to the equation: -

$$\underset{\text{Solid quartz}}{SiO_2} + \underset{\text{Alkaline aqueous}}{4NaOH} \longleftrightarrow \underset{\text{Soluble Na-silicates}}{Na_4SiO_4} + 2H_2O \quad \ldots\ldots(1)$$

These soluble silicates may react with the primary plagioclase to produce albite and secondary silica according to the following equation:-

$$\underset{\text{Solid anorthite}}{2CaAl_2Si_2O_8} + \underset{\text{Soluble Na-silicates}}{Na_4SiO_4} + 8O_2 \longleftrightarrow \underset{\text{Albite}}{4NaAlSi_3O_8} + \underset{\text{Secondary silica}}{2SiO_2} + 2Ca^{2+} \quad \ldots\ldots(2)$$

The produced $Ca^{2+}$ ions of reaction (2) together with magnesium liberated due to muscovitization of biotite precursor, precipitate under the prevailing alkaline medium in the form of carbonates such as calcite, according to the following equations:-

$$Ca^{2+} + CO_3^{2-} \longleftrightarrow CaCO_3 \quad \ldots\ldots(3)$$
$$Mg^{2+} + 2CaCO_3 \longleftrightarrow CaMg(CO_3)_2 + Ca^{2+} \quad \ldots\ldots(4)$$

The oxidizing alkaline hydrothermal solutions will deteriorate the $Fe^{2+}$ bearing minerals such as biotite, according to the following equation:-

$$\underset{\text{Biotite}}{KMgFe_2(AlSi_3O_{10})(OH)_2} + 2Al(OH)_3 \longleftrightarrow \underset{\text{Muscovite}}{KAl_2\,AlSi_3O_{10})(OH)_2} + \underset{\text{Iron-oxy-hydroxide}}{2FeO(OH)} + Mg^{2+} \quad \ldots(5)$$

The produced iron oxide-hydroxide solidifies dehydrate into hematite that impart the altered granite with strong reddish brown hues. Most of the described alteration reactions reduce alkalinity and sudden change in the redox potential of the mineralizing solutions should have taken place upon oxidation of pre-mineralization sulfides (mostly of pyrite). At that stage, other oxidized chemical constituents, including uranium should have been reduced.

The formation of pyrite associated with pitchblende is depending on the abundance of $H_2S$ in the hydrothermal system (Eglizaud *et al.,* 2006). $H_2S$ can be enriched by the oxidation of the earlier pyrite according to the equations:

$$FeS_2 + 3H_2O \longrightarrow Fe^{2+} + S_2O_3^{\ 2-} + 6e- + 6H^+ \quad \ldots\ldots(6)$$
$$S_2O_3^{\ 2-} + H_2O \longrightarrow H_2S + SO_2^{\ 2-} \quad \ldots\ldots(7)$$

$Fe^{2+}$ and $Fe^{3+}$ will react with $H_2S$ to produce iron monosulfide (Hough *et al.,* 2019), while iron monosulfide is one of the direct reactants to produce authigenic pyrite (Yue *et al.,* 2019).

$$Fe^{3+} + O_2 + H_2S + CH_4 \longrightarrow SO_2^{-4} + FeS + CO_2 + H \quad \ldots\ldots(8)$$
$$Fe^{2+} + H_2S \longrightarrow FeS + 2H^+$$
$$FeS + H_2S \longrightarrow FeS_2 + H_2 \quad \ldots\ldots(9)$$

Simultaneously, $H_2S$ has a strong reduction capacity for uranyl, creating a strong reducing barrier for uranium precipitation (Liu *et al.,* 2017).

$$4UO_2^{+2} + H_2S + 10OH^- \longrightarrow 4UO^2 + SO_4^{2-} + 6H_2O \quad (10)$$

The other mineralizing stage is characterized by uranophane as the principal uranium mineral, which represents the secondary uranium mineralization in this occurrence. Uranophane either occurs locally overprinted pitchblende, or in a newly formed set of veins crosscutting hydrothermal fluorite. Uranophane is also associated with a series of alteration and gangue minerals mainly including calcite and fluorite. The mineralizing fluids were carbonate-rich, suggesting that uranium was transported as a uranyl carbonate complex.

## Acknowledgements

We are grateful to Prof. Dr. Mohamed Wetait, Prof. Dr. Zakaria Hamimi and Prof. Dr. Afaf Mahdy for providing their great knowledge and experience, which helped the authors to conduct this research. The authors thank Prof. Dr. Hassan El Sundoly, Prof. Dr. Ehab Abu Zeid, Prof. Dr. Adel El Afandy, Prof. Dr. Ahmed Abu Steet, Prof. Dr. Darweesh El Kholy, Prof. Dr. Mohsen Mohamadien Eng. Yehia Zakaria and Dr. Nasser Mahdy for their guidance and help. Also, authors are very much obliged to Prof. Dr. Ahmed Dardier and Prof. Dr. Hany Shalaby for providing useful advices and corrections.

## References

Abdel Hamid, A.A., 2006. Geologic Factors Controlling the Radon Emanation Associated with Uranium Mineralization along Wadi Belih, Ned., Egypt. M.Sc. Thesis, Benha University, 189.

Abu Zied, M.M., 1995. Relation between Surface and Subsurface Uranium Mineralization and Structural Features, Gebel Gattar, North Eastern Desert, Egypt. M.Sc. Thesis, Ain Shams University, 208.

Akaad, M.K. and A.M. Noweir, 1969. Lithostratigraphy of the Hammamt-Umm Seleimat District, Eastern Desert, Egypt. Nature, 223: 284-285.

Akaad, M.K. and A.M. Noweir, 1980. Geology and Lithostratigraphy of the Arabian Desert Orogenic Belt of Egypt between Latitudes $25^O 35^\backslash$ and $26^O 30^\backslash$N. Ins. Appl. Geol., king Abdul Aziz Univ., Jeddah, Bull., 3 (4): 127-135.

Burnham, C.W., 1962. Facies and Types of Hydrothermal Alteration. Economic Geology, 57: 768-784.

Chen, Z.Y. and Q.Y. Guo, 2007. Mechanism of U-Reduction and Concentration by Sulphides at Sandstone Type Uranium Deposits. Uranium Geology, 23: 321 – 327, 334.

Dawood, Y.H., 2003. Chemical Composition of Uranophane Associated with Peraluminous Granite, North Eastern Desert of Egypt. M.E.R.C. Ain Shams University, Earth Science Series, 17: 43-57.

Eglizaud, N., F. Miserque and E. Simoni, *et al.,* 2006. Uranium (VI) Interaction with Pyrite ($FeS_2$): Chemical and Spectroscopic Studies. Radiochimica Acta, 94:651– 656.

El Kammar, A.M., A.B. Salman, M.H. Shalaby and A.I. Mahdy, 2001. Geochemical and Genetical Constraints on Rare Metals Mineralization at the Central Eastern Desert of Egypt. Geochemistry Journal, 35: 117-135.

El Kholy, D.M., M.O. El Husseiny, W.H. Saleh and M.A. El Zalaky, 2012. Remote Sensing, Geology and Geochemistry on the GVIII Uranium Mineralization, Gabal Gattar, North Eastern Desert, Egypt. Nuclear Sciences Scientific Journal, 1: 69-84.

El Kholy, D.M., H.A. Khamis and H.L. El Sundoly, 2019. Geology and Structural Relationship between Uranium Occurrences in the Northern Part of Gabal Gattar, Northern Eastern Desert, Egypt. Nuclear Sciences Scientific Journal, 8A: 1–18.

El Rakaiby, M. L. and M.H. Shalaby, 1988. Geology of Gabal Qattar Batholith, central Eastern Desert, Egypt. International Journal of Remote Sensing, 13: 2337-2347.

El Ramly, M.F. and M.K. Akaad, 1960. The Basement Complex in the Central Eastern Desert of Egypt between Latitudes $24^0 30^\backslash$ and $25^0 40^\backslash$ N. Annals of the Geological Survey of Egypt, Paper 8, 35.

El Sundoly, H.I. and A.G. Waheeb, 2015. A New Genetic Model for the Localization of Uranium Minerals at the Northern Part of Gabal Gattar, North Eastern Desert, Egypt. Third Symposium of the Geological Resource in the Tethys Realm, Cairo Univ., 21-39.

Seimbille, F., P. Zuddas and M. Gil, 1998. Granite–Hydrothermal Interaction: A Simultaneous Estimation of the Mineral Dissolution Rate Based on the Isotopic Doping Technique. Earth and Planetary Science Letters, 157: 183–191.

Haridy, M.H., 1995. Physical and Mechanical Properties of Gabal Gattar Granitic Pluton and the Relation to Joint-Type U-Mineralization. M.Sc. Thesis, Cairo University, 172.

Holail, H.M., and A.M. Moghazi, 1998. Provenance, Tectonic Setting and Geochemistry of Greywackes and Siltstones of the Late Precambrian Hammamat Group, Egypt. Sedimentary Geology, 116: 227-250.

Hough, G., S. Swapp and C. Frost, *et al.,* 2019. Sulfur Isotopes in Biogenically and Abiogenically Derived Uranium Roll-Front Deposits. Economic Geology, 114: 353 – 373.

Khalaf, M.A., 1995. Petrological and Mineralogical Characteristics of Some Uranium Bearing Younger Granites, North Eastern Desert, Egypt. M.Sc. Thesis, Cairo University, 78.

Khazback, A.E., M.H. Shalaby and M.F. Raslan, 1995. On the Occurrence of Some Secondary Uranium Minerals and Fluorite in Gabal Gattar Locality, Eastern Desert, Egypt. Egyptian Mineralogist, 7: 47-63.

Krauskopf, K., 1982. Introduction to Geochemistry, McGraw-Hill Book Company, New York, 721.

Langmuir, D., 1978. Uranium Solution-Mineral Equilibria at Low Temperatures with Applications to Sedimentary Ore Deposits. Geochimica et Cosmochimica Acta, 42: 547 – 569.

Liu, W.S., X.Q. Zhao and Q.P. Shi, *et al.,* 2017. Research on Relationship of Oil-Gas and Sandstone-Type Uranium Mineralization of Northern China. Geology in China, 44: 279 – 287.

Mahdy, A.I., 1999. Petrological and Geochemical Studies on the Younger Granites and Hammamat Sediments at G-V Uranium Occurrence, Wadi Bali, North Eastern Desert, Egypt. Ph.D. Thesis, Ain Shams University, 198.

Mahdy, M.A., A.B. Salman and A.H. Mahmoud, 1990. Leaching Studies on the Uraniferous Hammamat Sediments, Wadi Belih, Northern Eastern Desert, Egypt, 14th Congress of Mining and Metallurgy, Edinburgh Scotland, 229-235.

Mahdy, N.M., M.H. Shalaby, H.M. Helmy, A.F. Osman, E.H. El Sawey and E.K. Abu Zeid, 2014. Trace and REE Element Geochemistry of Fluorite and Its Relation to Uranium Mineralizations, Gabal Gattar Area, Northern Eastern Desert, Egypt. Arabian Journal of Geoscience, 7: 2573–2589.

Mahdy, N.A., B.A. El Kalioubi, C.C. Wohlgemuth-Ueberwasser, M.H. Shalaby and A.H. El Afandy, 2015. Petrogenesis of U- And Mo-Bearing $A_2$-Type Granite of the Gattar Batholith in the Arabian Nubian Shield, Northeastern Desert, Egypt: Evidence for the Favorability of Host Rocks for the Origin of Associated Ore Deposits. Ore Geology Review, 71: 57–81.

Raslan, M.F., 2009. Occurrence of Uraniferous Iron Grains at Gabal Gattar, El Missikat and El Erediya Granites in Eastern Desert of Egypt. Resource Geology, 59: 99–105.

Rich, R.A., H.D. Holland and U. Petersen, 1977. Hydrothermal Uranium Deposits. Elsevier Science, New York.

Roz, M.E., 1994. Geology and Uranium Mineralization of Gabal Gattar Area, North Eastern Desert, Egypt. M.Sc. Thesis, Al Azhar University, 175.

Sayyah, T.A. and M.Y. Attawiya, 1990. Contribution to the Mineralogy of Uranium Occurrence of Gebel Gattar Granites, Eastern Desert, Egypt. Arabian Journal of Nuclear Science, 23: 171-184.

Shahin, H.A., 2014. Geochemical Characteristics and Chemical Electron Microprobe U-Pb-Th Dating of Pitchblende Mineralization from Gabal Gattar Younger Granite, North Eastern Desert, Egypt. Open Journal of Geology, 4: 24-32.

Shalaby, M.H., 1990. Uranium Mineralization in the Northern Gabal Qattar Locality, Northern Eastern Desert.7th Conf. Phanerozoic and Developement, Al Azhar University, 3: 19.

Shalaby, M.H., 1995. New Occurrence of Uranium Mineralization, G-VII, Gabal Qattar Uranium Prospect, North Eastern Desert, Egypt. Bulletin of the Faculty of Science, Alexandria University, 35: 447– 460.

Shalaby, M.H., 1996. Structural Controls of Uranium Mineralizations at Gabal Qattar, North Eastern Desert, Egypt. Proceeding of the Egyptian Academy of Science, 46: 521-536.

Yue, L., Y.Q. Jiao and L.Q. Wu, *et al.,* 2019. Selective Crystallization and Precipitation of Authigenic Pyrite during Diagenesis in Uranium Reservoir Sand Bodies in Ordos Basin. Ore Geology Reviews, 107: 532– 545.